RSC Advances

PAPER

View Article Online
View Journal | View Issue

Cite this: *RSC Adv.*, 2026, **16**, 28103

Spontaneous self-assembly of mangiferin in an aqueous medium into vesicles for anticancer drug encapsulation and antibacterial applications

Sukhendu Kar,[a] Soumen Patra,[a] Wachirasak Thaisaeng,[b] Chatphorn Theppitak,[b] Nopporn Thasana*[bcd] and Braja Gopal Bag *[a]

Natural products exhibiting spontaneous vesicular self-assembly are rare. Mangiferin, a natural xanthonoid, was isolated from the rhizome of the fern *Davallia solida*. Herein, we demonstrate that mangiferin spontaneously self-assembles in aqueous and organic-aqueous binary solutions, forming stable spherical vesicles. The morphology of these self-assemblies was confirmed using optical microscopy, atomic force microscopy, scanning electron microscopy, high-resolution transmission electron microscopy, FTIR spectroscopy and X-ray diffraction studies. The critical vesicular concentrations determined in DMSO–water (2 : 1 v/v and 1 : 1 v/v) and water alone using pyrene as a fluorescence probe were 60 μM, 50 μM and 30 μM, respectively. The resulting mangiferin vesicles were successfully utilized for the encapsulation of various molecules, including the anticancer drugs doxorubicin and curcumin. The therapeutic potential of the system was demonstrated by two applications. First, the mangiferin vesicles successfully encapsulated doxorubicin, confirming their role as a prospective drug delivery system. Second, the curcumin-loaded mangiferin vesicles exhibited significantly enhanced antibacterial activities against both the Gram-positive (*Staphylococcus aureus*) and Gram-negative (*Escherichia coli*) bacteria compared with free curcumin dissolved in a DMSO–water system. Thus, this study introduces a natural product-derived vesicular nanocarrier based on the spontaneous self-assembly of mangiferin, highlighting its significant potential as a biologically and medicinally important carrier system for dual-drug delivery and anti-infective applications.

Received 14th February 2026
Accepted 4th May 2026

DOI: 10.1039/d6ra01279e

rsc.li/rsc-advances

1. Introduction

Self-assembly is a fundamental process where a disordered system spontaneously forms an ordered, organized structure based on specific, intrinsic interactions among its components, without the need for external forces.[1,2] When these components are molecules, the process is termed molecular self-assembly.[3] This process is driven by weak, noncovalent interactions, such as van der Waals forces, hydrogen bonding, solvophobic, electrostatic, and aromatic–aromatic interactions.[4–6] Examples of molecular self-assembly include the formation of crystals and polymers, as well as colloidal structures, such as fibers, tubes, monolayers and vesicles.[7–11] The resulting organized assemblies have broad applications in nanoscience, nanotechnology, bio-nanotechnology and vaccine development.[12–14]

The self-assembly of natural products has gained significant interest in recent years because of their diversified molecular frameworks and functional groups and also their availability in renewable supply without any extensive synthetic efforts.[5,15–17] Previously, we have reported the self-assembly of terpenoids having diversified structural frameworks and functional groups in liquids.[5,18] Minute structural variation and the functional group dispositions have resulted in different morphologies *via* the hierarchical self-assembly of terpenoids in different liquids. Mangiferin (MGF) is a naturally occurring polyphenolic xanthonoid (Fig. 1). Its structure is defined by a xanthone backbone, a secondary metabolite found in fungi, lichens and higher plants, and a glucoside unit.[19–22] MGF is widely isolated from various plant sources, including the bark, leaves, kernels and peels of the mango tree (*Mangifera indica*), as well as the leaves of *Bombax ceiba* and coffee plants.[23–27] Notably, young *M. indica* leaves contain a higher concentration of MGF than older leaves and bark.[28] MGF exhibits numerous pharmacological and biological activities, making it a molecule of significant interest. These activities include anti-diabetic, uric acid reduction, anti-inflammatory and anti-oxidative effects.[29–32] Furthermore, it

[a]*Department of Chemistry and Chemical Technology, Vidyasagar University, Midnapore 721102, West Bengal, India. E-mail: brajagb@gmail.com*
[b]*Laboratory of Medicinal Chemistry, Chulabhorn Research Institute, Laksi, Bangkok 10210, Thailand*
[c]*Program of Chemical Sciences, Chulabhorn Graduate Institute, Laksi, Bangkok 10210, Thailand*
[d]*Center of Excellence on Environmental Health and Toxicology (EHT), OPS, Ministry of Higher Education, Science, Research and Innovation, Bangkok 10400, Thailand*

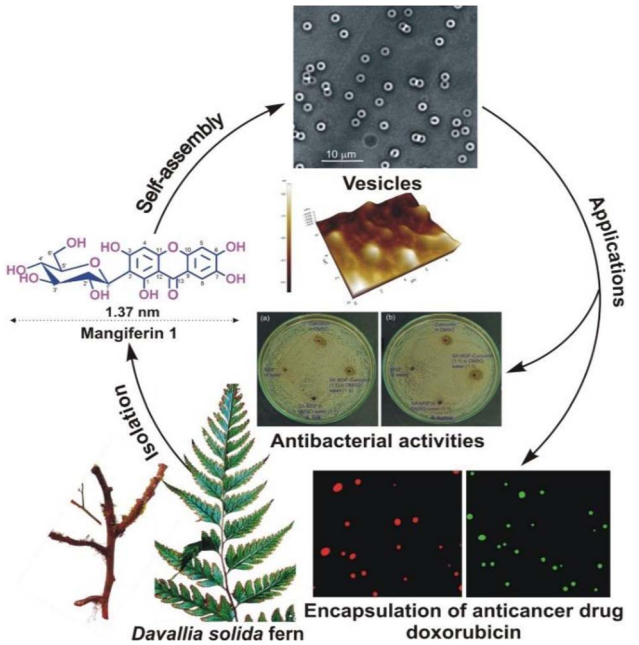

Fig. 1 Schematic representation of the self-assembly of mangiferin (MGF) **1** extracted from the dried rhizome of the fern *Davallia solida* yielding vesicles, its use in the entrapment of the anticancer drug doxorubicin and its antibacterial activities.

demonstrates antimicrobial, antiviral and anticancer properties,[33–36] and has applications in the cosmetic industry.[37] Structurally, the presence of a C-glycosyl linkage and multiple aliphatic and aromatic polyhydroxy groups contribute significantly to its free radical scavenging and antioxidant potential. MGF absorption primarily occurs in the small intestine *via* passive diffusion through the gastrointestinal tract.[22] However, a major limitation to the medicinal application of MGF is its poor solubility in water, which translates to low bioavailability in biological systems. Although it is completely soluble in organic solvents like dimethyl sulfoxide (DMSO), a solvent suitable for various biological and pharmaceutical applications, its poor aqueous solubility remains a challenge.

Structurally mangiferin (MGF) has a C-glycosidic linkage but there are other flavonoid glycosides such as rutin and hesperidin that have O-glycosidic linkages, which are easily hydrolyzable. This carbon–carbon bond between the xanthone nucleus and the glucose moiety makes MGF highly stable against acid hydrolysis and enzymatic degradation in the digestive tract, allowing it to reach the lower intestine largely intact. Like many polyphenols, MGF has poor bioavailability (<2%). While many glycosylated polyphenols, like quercitin, are studied for general antioxidant effects, MGF is specifically recognized for significant neuroprotective effects (Alzheimer's and Parkinson's) and strong antidiabetic, antitumor (prostate, breast, lung, and ovarian), and hepatoprotective properties.[38,39]

To address the low aqueous solubility and bioavailability of MGF, we investigated its self-assembly behaviour using organic-aqueous binary solvent systems.[40,41] Herein, we report the first observed vesicular self-assembly of mangiferin in organic-aqueous binary liquids. Spontaneous formation of vesicular self-assemblies was observed, even in water alone. The resulting spherical vesicular objects were characterized using various microscopic and spectroscopic techniques, including optical microscopy (OM), atomic force microscopy (AFM), scanning electron microscopy (SEM), high-resolution transmission electron microscopy (HRTEM), Fourier-transform infrared (FTIR) spectroscopy and X-ray diffraction (XRD). The utility of these vesicular self-assemblies was demonstrated through the successful entrapment of various fluorophores (rhodamine-B and carboxyfluorescein) and the anticancer drugs (doxorubicin and curcumin), followed by the controlled release of the fluorophores from the vesicular cavity. Our findings show that the vesicular self-assembly of MGF significantly increases its solubility and bioavailability. Furthermore, curcumin-loaded self-assembled MGF showed enhanced antibacterial activity against both Gram-positive (*Staphylococcus aureus*) and Gram-negative (*Escherichia coli*) bacteria in a DMSO–water (1 : 1 v/v) system compared to curcumin alone.

2. Results and discussion

Mangiferin ($C_{19}H_{18}O_{11}$) is a natural polyphenolic xanthonoid containing the xanthone backbone and a glucoside unit (Fig. S1). The length of the molecule is 1.37 nm calculated by DFT using the Gaussian 09 software and PC MODEL® using MMX force field (Fig. S2 and S3).[42,43] The molecule has a flat tricyclic xanthone ring system containing both polar hydroxyl groups and lipophilic part. The HLB value calculated by the Griffin method is 9.28, suggesting a potential for self-assembly in aqueous media (Table TS1). The HLB value 9.28 predicts the formation of vesicles rather than micelles or aggregates because it falls within a specific, intermediate range, generally 4–10, which indicates a balance between hydrophilicity and lipophilicity, making it ideal for the formation of vesicles rather than spherical micelles or simply dispersed aggregates. MGF was isolated from the dried rhizome of *Davallia solida* fern and characterized by various spectroscopic techniques (see Experimental section 5).

2.1 Study of self-assembly properties

For self-assembly studies, MGF (2 mg) contained in a vial (capacity 4 mL) was dissolved in a liquid under hot conditions with stirring and then allowed to cool at room temperature and observed visually and under an optical microscope (see Experimental section 5.1.3). For studying the self-assembly in binary liquid mixtures, MGF (2 mg) was dissolved initially in an organic liquid like DMSO under hot conditions and then the clear solution was gradually treated with water until cloudiness appeared. It was re-dissolved by heating, allowed to cool and then observed. We observed the key differences in the physical state of MGF depending on the solvent system and concentration (Table 1).

2.1.1 Aqueous media. At the highest concentration tested in water (16.57 mM), MGF initially formed a white colloidal solution. However, this colloidal solution was unstable and led to the precipitation of a white solid over time. At lower

Table 1 Self-assembly studies of MGF (**1**) in neat organic liquids and organic-aqueous binary liquid mixtures

Entry	Medium (v/v)	Conc (mM)	State[a]
1	Water (H_2O)	16.57	CS
2	H_2O	2.00	VS
3	H_2O	1.00	VS
4	DMSO	2.00	S
5	DMSO	63.14	VS
6	DMSO–H_2O (2 : 1)	31.57	VS
7	DMSO–H_2O (1 : 1)	17.36	VS
8	DMSO–H_2O (1 : 1)	2.00	VS
9	DMSO–H_2O (1 : 2)	2.00	VS
10	THF	2.00	CS
11	THF	56.82	VS
12	THF–H_2O (1 : 1)	2.00	VS
13	EtOH	2.00	S
14	EtOH	86.82	VS
15	EtOH–H_2O (1 : 1)	2.00	VS
16	DMF	2.00	S
17	DMF–H_2O (2 : 1)	31.57	VS

[a] CS = colloid solution, VS = viscous suspension, and S = soluble (clear solution).

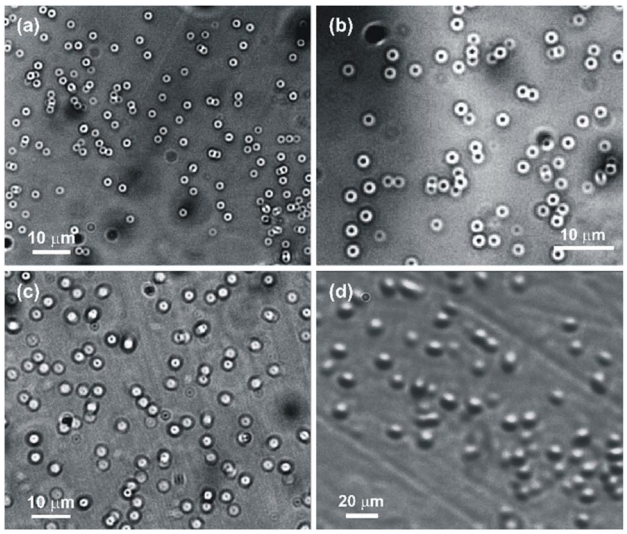

Fig. 2 Optical microscopy images of MGF (**1**) in (a and b) DMF–H_2O (2 : 1 v/v, 31.6 mM), (c) DMSO–H_2O (1 : 1 v/v, 17.4 mM) and (d) DMSO–H_2O (1 : 2 v/v, 2 mM).

concentrations (1.00 mM and 2.00 mM, entries 2 and 3, Table 1), MGF formed a viscous suspension.

2.1.2 Neat organic solvents. MGF formed clear solutions (S) at low concentrations in DMSO, EtOH and DMF. In THF, a colloidal solution (C.S) was observed at low concentrations. At higher concentrations in neat organic liquids (DMSO, THF and EtOH), MGF formed a viscous suspension (VS).

2.1.3 Organic-aqueous mixtures. Critically, MGF consistently formed a viscous suspension (VS) across all tested organic-aqueous binary mixtures, including DMSO–H_2O, THF–H_2O, EtOH–H_2O and DMF–H_2O.

The formation of colloidal solutions and viscous suspensions in both neat organic solvents (at high concentrations) and mixed aqueous systems strongly suggests the spontaneous formation of molecular self-assemblies driven by solvophobic effects with additional non-covalent interactions.

2.2 Characterization of morphology of the self-assemblies

Aliquots of the stable colloidal and viscous suspension samples were collected for detailed morphological investigation. The morphologies of the self-assembled MGF (**1**) in different neat solvents and organic-aqueous binary solvent mixtures were characterized by optical microscopy, atomic force microscopy (AFM), scanning electron microscopy (SEM), high-resolution transmission electron microscopy (HRTEM) and Fourier transform infrared (FTIR) spectroscopy.

2.2.1 Optical microscopic studies. Vesicles are recognized as a biologically effective system for drug delivery and cellular processes. The self-assembly morphology of MGF (**1**) was investigated using optical microscopy. Samples were prepared by placing the self-assembled solutions in their native state over glass slides and covering them with coverslips. Interestingly, spherical objects were observed in both neat solvents (such as DMSO) and organic-aqueous binary solvent mixtures DMSO–H_2O, DMF–H_2O and pure water at lower concentrations. These spherical objects were identified as vesicles (Fig. 2 and S4). While typically described in cell biology as small sacs enclosed by a lipid bilayer that form naturally, we successfully prepared these vesicles in the laboratory. The micrometer seized vesicles were observed in the optical microscopy in DMSO (63.14 mM), DMSO–H_2O (1 : 1 v/v, 17.36, 2 mM), DMSO–H_2O (1 : 2, 2 mM), DMF–H_2O (2 : 1 v/v, 31.57 mM) and only water (1 mM, 2 mM) at lower concentrations (Fig. 2 and S5). The micro-meter-sized vesicular objects have an average diameter of 2.36 μm, 3.78 μm and 9.89 μm in DMF–H_2O (2 : 1 v/v, 31.57 mM), DMSO–H_2O (1 : 1 v/v, 17.36 mM) and water (1 mM), respectively (Fig. S5). Nano-sized spherical objects could not be observed due to the limitation of optical microscopy. Due to this limitation of optical microscopy, which prevents the observation of nano-sized spherical objects, further insights into the morphology of the assemblies were obtained using atomic force microscopy (AFM), scanning electron microscopy (SEM), and high-resolution transmission electron microscopy (HRTEM).

2.2.2 AFM studies. Atomic force microscopy (AFM) was used to gain high-resolution topographical insights into the morphology of the self-assemblies, providing resolution orders of magnitude better than the optical diffraction limit. The high-resolution AFM imaging provided detailed two-dimensional (2D) and three-dimensional (3D) topological maps (Fig. 3 and S6). The spherical objects were observed interestingly from the dried self-assemblies of MGF in the DMSO–H_2O system (1 : 1 v/v, 2 mM) with high resolution of 2D and 3D topological images by atomic force microscopy. The diameter range of the spherical objects was 500 nm–2 μm and the average diameter was 1.34 μm, and the heights of the spherical objects were 5–80 nm (Fig. 3 and S6). The line profile analysis (Fig. 3c) confirmed these dimensions. This flattened morphology suggests that the vesicular structures may have collapsed or spread upon deposition and drying on the surface.

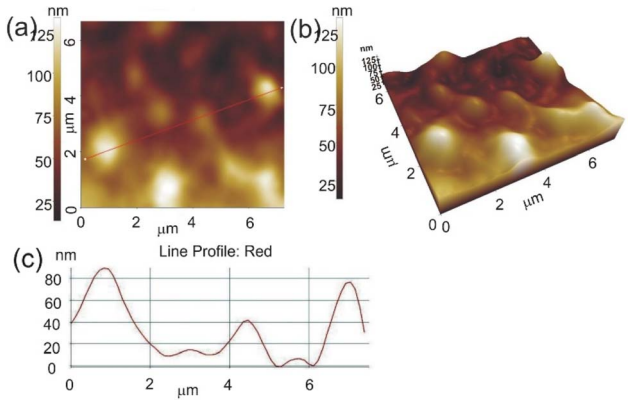

Fig. 3 AFM images of the dried self-assemblies of MGF (**1**) in DMSO–H_2O (1 : 1 v/v, 2 mM). (a) 2D image of the vesicular self-assemblies, (b) 3D image of the vesicular self-assemblies and (c) line profile of the spherical object drawing.

2.2.3 SEM studies. Scanning electron microscopy (SEM) was used to confirm the overall morphology and size of the self-assembled structures. The self-assemblies of MGF, prepared in pure water at a lower concentration (1 mM), exhibited distinct vesicular self-assemblies. The SEM images confirm the presence of spherical objects (Fig. 4 and S7). Quantitative analysis revealed that these vesicles were on the nanoscale, with an average diameter of 300 nm. The slight variations in the observed shape of the assemblies are likely a consequence of the complex solvent–solute interactions changing with the concentration and the inherent soft nature of the assemblies, which may lead to some structural distortion upon drying for the SEM analysis.

2.2.4 HRTEM studies. High-Resolution Transmission Electron Microscopy (HRTEM) was performed to observe the nanoscale morphology and determine the wall thickness of the self-assembled structures. The colloidal solutions of MGF, prepared in organic-aqueous solvent mixtures like DMF–water (2 : 1 v/v, 3 mM) and DMSO–water (1 : 1 v/v, 2 mM), were cast onto TEM grids and analyzed. HRTEM confirmed the presence of vesicular morphology (Fig. 5 and S8). Crucially, the observed membrane thickness of the vesicular self-assemblies was measured to be 2.74 nm. This thickness is approximately twice the calculated molecular length of mangiferin (1.37 nm). This key observation supports the formation of a bilayer vesicular morphology for the self-assemblies of MGF. The presence of dark-colored spherical areas in some HRTEM images is characteristic of the soft nature of the MGF vesicular self-assemblies.

2.2.5 FTIR studies. FTIR spectroscopy was employed to probe the nature of non-covalent interactions, specifically H-bonding, which drives the self-assembly of MGF. We compared the spectra of the neat MGF powder with the MGF self-assemblies formed in DMF–water (2 : 1 v/v, 31.57 mM) (Fig. S9). The key observation is the shift in the hydroxyl O–H stretching frequency. The O–H stretching peak in the neat MGF powder appeared at 3358 cm^{-1} whereas, this peak shifted slightly to 3363 cm^{-1} in the self-assembled structure (in DMF–water). This small but observable blue-shift (+5 cm^{-1} increase in frequency) for the O–H groups suggests a change in the strength or geometry of the intermolecular hydrogen bonds involving the hydroxyl groups upon self-assembly. Crucially, the stretching frequency of the carbonyl C=O groups remained unchanged at 1655 cm^{-1} in both the neat powder and the self-assembled structure. This might be due to the fact that the extent of H-bonding of the C=O group is identical both in the neat powder sample and the self-assemblies of MGF. Therefore, the FTIR results support the hypothesis that inter-molecular hydrogen bonding between the multiple O–H groups of

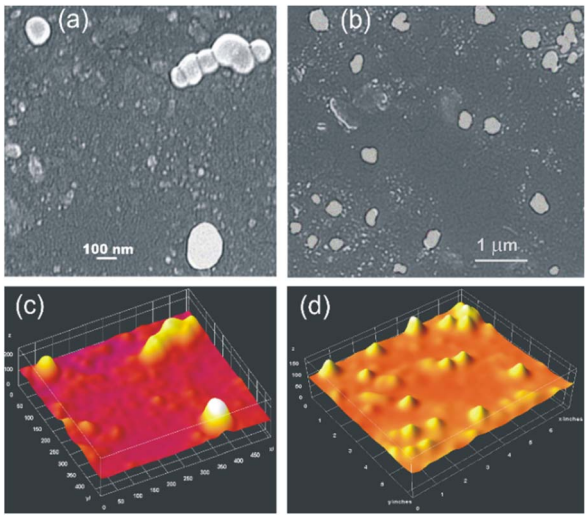

Fig. 4 SEM images of the dried self-assemblies of MGF (**1**) in H_2O (1 mM) giving spherical objects (vesicles) at lower concentrations: (a and b) 2D images and (c and d) 3D images, generated using the ImageJ software.

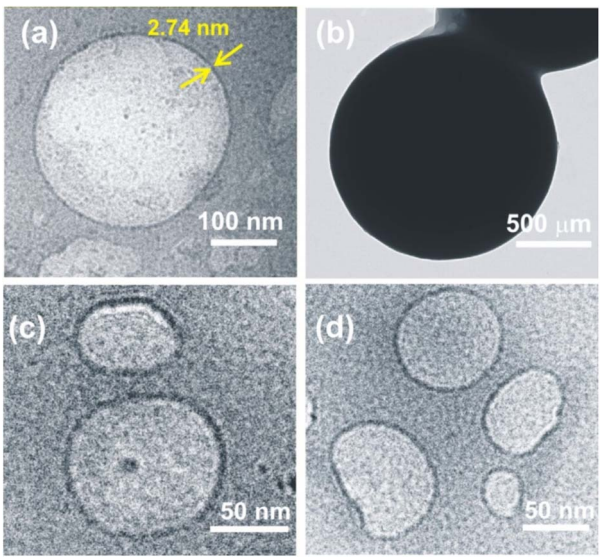

Fig. 5 HRTEM (without staining) images of the vesicles from MGF self-assembled in (a and b) DMF–water (2 : 1 v/v, 3 mM) and (c and d) in DMSO–water (1 : 1 v/v, 2 mM) systems.

adjacent MGF molecules is a significant driving force for the formation of the self-assembled structures.

2.2.6 Powder X-ray diffraction studies. Powder X-ray diffraction was conducted at room temperature using a Bruker D6 PHASER X-ray diffractometer. Data were collected and integrated over a 2θ range of 5–50° with a step size of 0.02°, utilizing the Bruker software. The simulated powder patterns were generated from single-crystal X-ray diffraction data and processed using the Mercury software,[44] which were provided by the Cambridge Crystallographic Data Centre (CCDC).[45] The PXRD patterns of commercial MGF and MGF from *Davallia solida* were compared with the simulated pattern,[46] demonstrating a good match in their phase purity (Fig. S10). The crystal structure of MGF in H_2O solvents has been reported by Jose W Cruz Jr. and co-workers (Fig. S11).[47] Experimental PXRD patterns obtained for the dried self-assemblies of MGF obtained from DMSO (green), DMSO–H_2O (2 : 1 v/v) (deep blue), and DMSO–H_2O (1 : 1 v/v) (violet) were also compared (Fig. S10). Most of the peaks obtained from the self-assemblies were identical, indicating that these samples have identical ordered structures.

2.2.7 Dynamic light scattering (DLS) studies. DLS measurements carried out with self-assembled MGF in water alone showed an increase in the size of the self-assemblies from 164, 246 to 752 nm, respectively, with the increase in concentrations from 0.1 mM, 1 mM to 2 mM (Fig. S12). Identical experiments carried out with self-assembled MGF in DMSO–water (1 : 1 v/v) also showed an increase in the size of the self-assemblies having poly-disperse nature from 127 to 476 nm (Fig. S13). Although the PDI values were higher in water alone (PDI = 1), much lower PDI values (0.324, 0.722 to 0.782) were observed in DMSO–water (1 : 1 v/v), indicating the stability of the self-assembled vesicles. Such polydisperse nature has also been observed by various microscopic techniques. DLS studies carried out with a freshly prepared sample of self-assembled MGF in DMSO–water (1 : 1 v/v, 0.1 mM) at the time intervals of (a) 10 min, (b) 20 min and (c) 30 min (Fig. S14) did not show any significant change in the sizes of the self-assemblies. Identical experiments carried out with a freshly prepared sample of self-assembled MGF in water alone (0.1 mM) also did not show any significant change in the sizes of the self-assemblies (Fig. S15).

2.2.8 Critical vesicular concentration (CVC) studies. The Critical Vesicular Concentration (CVC) values of mangiferin were determined using pyrene as a fluorescence probe in a DMSO–water (1 : 1 v/v) binary liquid mixture. At first, 20 vials were prepared, each of them containing 1.0 μM pyrene and 0.01–0.20 mM of mangiferin and added certain amounts of DMSO solvent and distilled water to maintain the DMSO–water (1 : 1 v/v) solvent system. Then fluorescence spectroscopy studies were performed with the excitation wavelength at 335 nm and the values of I_1 and I_3 were obtained at the wavelengths 375 nm and 385 nm, respectively. The CVC value of mangiferin obtained in the DMSO–water (1 : 1 v/v) solvent system was 50 μM (Table TS2 and Fig. S16). Similarly, the CVC value of MGF obtained in the DMSO–water (2 : 1 v/v) solvent system was 60 μM (Table TS2 and Fig. S17). Interestingly, the CVC value of MGF obtained in water was 30 μM (Table TS2 and Fig. S18). The decrease in CVC values with the increasing percentage of water is due to the lower solubility of the compound in water. This observation is in tune with the previous reports from our laboratory with terpenoid-based vesicular self-assembles.[9,48]

2.3 Proposed model for molecular self-assembly

Mangiferin (MGF) is a polyphenolic xanthonoid containing the xanthone backbone and a glucoside unit. The inter-molecular hydrogen bonding among the –O–H groups occurs in the vesicular self-assemblies, which was confirmed by the FTIR studies. H-bonding interactions among various '–O–H' groups of MGF were observed in the crystal packing of MGF (Fig. S11). The molecular length of MGF obtained from the DFT calculation and the PC model was 1.37 nm. The membrane thickness of the vesicular self-assemblies obtained from HRTEM studies is 2.74 nm, which is twice the molecular length of MGF (1.37 nm). This indicates that MGF forms bilayer vesicles in liquids *via* a hierarchical self-assembly. The MGF molecule may be considered as a 'bola'-amphiphile having unsymmetrical polar and nonpolar regions. The mechanism of the formation of bilayer vesicles from such amphiphiles has been described in detail in the literature.[13,49] Bilayer vesicles may result when the packing parameter ($P = V/a_0l_c$) falls in the range of $1/2 < P < 1$.[49] Two MGF molecules can form a dimer *via* H-bonding, leading to a bilayer vesicular self-assembly, as shown in Fig. 6.[50,51] The void space inside the vesicular self-assemblies, as shown in the 2D-bilayer and 3D vesicular models and the HRTEM image (Fig. 6e, f and g, respectively), can be utilized for the entrapment of various molecules including drugs. It has been discussed in the following sections.

3. Utilization of vesicular self-assemblies

3.1 Entrapment of several fluorophores including anticancer drug doxorubicin inside the vesicular self-assemblies of mangiferin

Vesicular self-assemblies are suitable for targeted drug delivery through blood capillaries.[52–54] To determine whether the vesicular self-assemblies of MGF are capable of entrapping guest molecules inside, we examined the entrapment of rhodamine B (Rho-B), anticancer drug doxorubicin (DOX) and an anionic fluorophore 5,6-carboxy-fluorescein (CF). Interestingly, the bright red and green fluorescence was observed from the inner side of the vesicular self-assemblies under green and blue emission light, respectively, indicating the entrapment of the fluorophores and anticancer drug doxorubicin inside the vesicles (Fig. 7 and 8a). When a hot solution of mangiferin in DMSO–water (1 : 1 v/v, 17.36 mM) containing the anticancer drug Dox (1 mM) was cooled to room temperature and examined by epifluorescence microscopy, bright green and red fluorescence was observed from the inner side of the vesicular self-assemblies under blue and green emission light, respectively, indicating the entrapment of doxorubicin inside the vesicles (Fig. 7a and b).

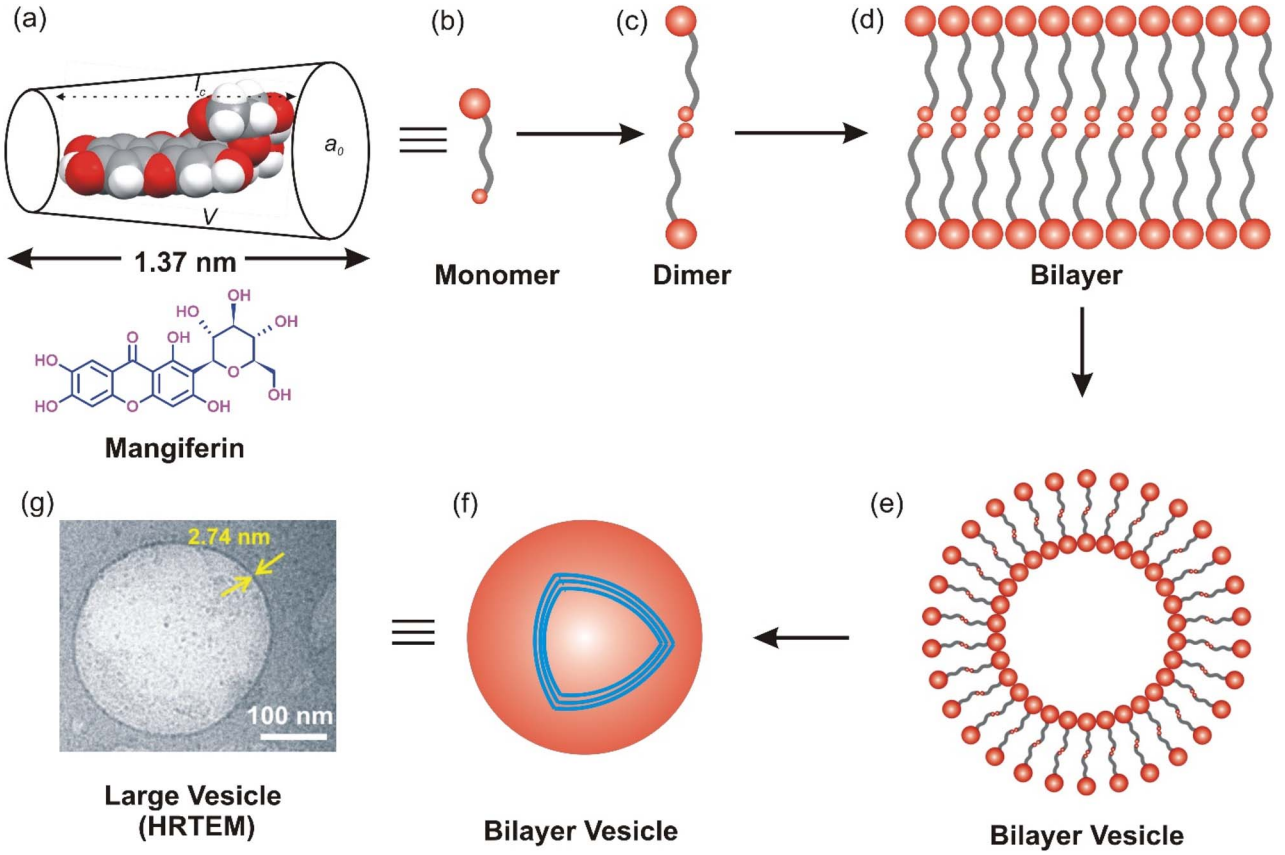

Fig. 6 Schematic representation of the formation of bilayer vesicles from MGF. (a) Space-fill structure of MGF; where V and l_c are the volume and the length of the hydrophobic part, respectively, and a_0 is the cross-sectional area of the hydrophilic part of the amphiphile. (b) Monomer of MGF, with the head group formed with the polar glucoside unit and the tail group formed with the nonpolar flat tricyclic xanthone ring system. (c) Dimer of MGF. (d) Bilayer formed with the more polar head group in the exterior. (e and f) Formation of the bilayer vesicle. (g) HRTEM image of the vesicles.

Similarly, the bright green fluorescence was observed from the inner side of the vesicular self-assemblies under blue emission light, indicating the entrapment of the anionic fluorophore 5,6-carboxy-fluorescein (CF) inside the vesicles (Fig. 7d). When a hot solution of mangiferin in DMSO–water (1 : 1 v/v, 14.99 mM) containing rhodamine B (Rho-B) (0.15 mM) was cooled to room temperature and examined by epi-fluorescence microscopy, bright red fluorescence was observed inside the spheres under green emission light, indicating the entrapment of Rho-B inside the vesicles (Fig. 7c and 8a). The entrapment of Rho-B was also studied by fluorescence emission experiments using a fluorimeter, and the fluorescence emission intensities were measured at different time intervals after excitation at 510 nm. A gradual decrease in the intensities of fluorescence emission was observed, indicating the entrapment of the Rho-B inside the vesicles (Fig. 8c). From the plot of intensity *vs.* wavelength (Fig. S14a), we calculated the value of percentage entrapment of rhodamine-B as 28.8% by the vesicular self-assemblies of MGF within 160 min (Fig. S19a).

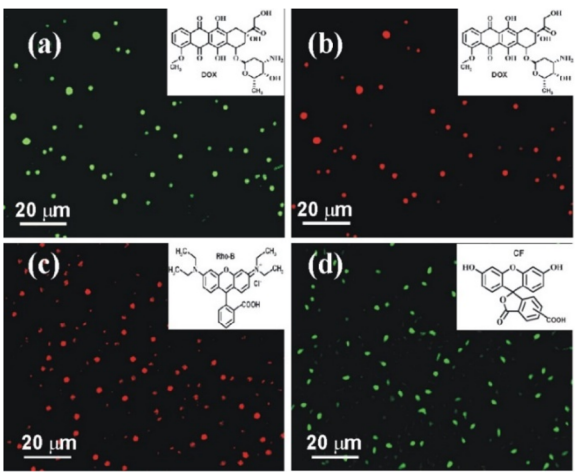

Fig. 7 Epifluorescence microscopy images of mangiferin in DMSO–water (1 : 1 v/v): (a and b) entrapped doxorubicin (17.36 mM MGF and 1 mM Dox), (c) entrapped Rho-B (14.99 mM MGF and 1 mM Rho-B) and (d) entrapped CF (14.99 mM MGF and 3 mM CF).

3.2 Release of the entrapped toxic dye rhodamine-B (Rho-B) from the vesicular self-assemblies of mangiferin

The ability of the MGF vesicles to act as a functional encapsulation system was studied by the controlled release of the model toxic dye, rhodamine-B (Rho-B). Triton X-100, a non-ionic surfactant known to disrupt lipid bilayers by hydrogen

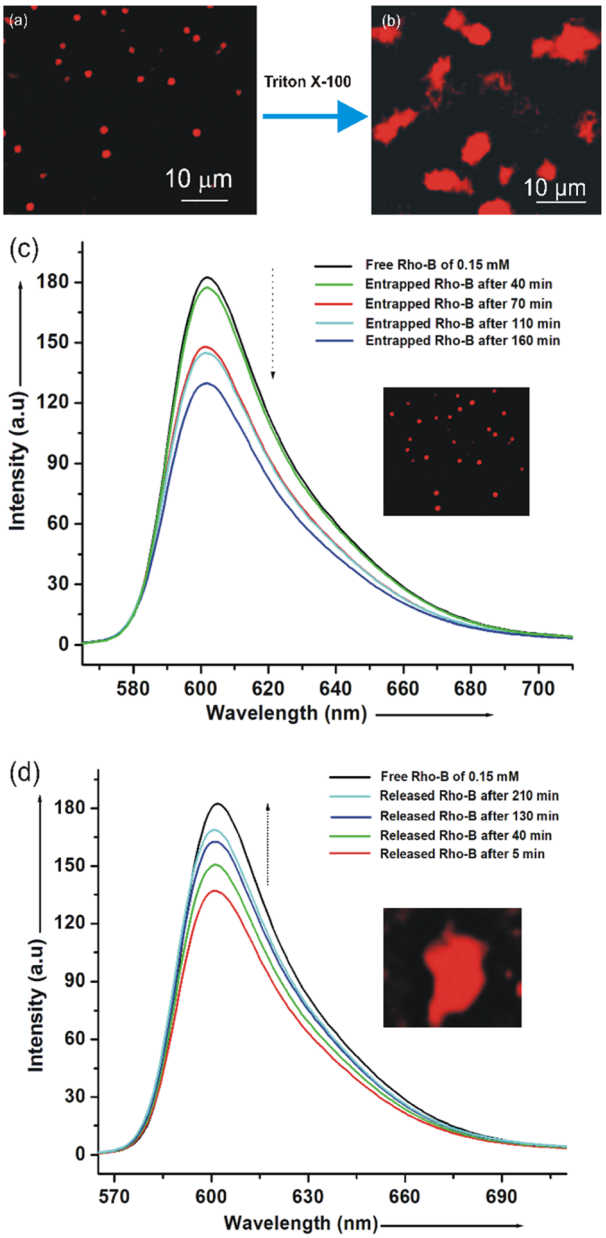

Fig. 8 Entrapment of Rho-B by the vesicular self-assemblies of MGF (**1**) and its release. (a) Fluorescence images of self-assembled **1** in DMSO–H_2O (1 : 1 v/v, 15 mM) containing Rho-B (0.15 mM) exposed under green emission light. (b) Fluorescence images on treatment with vesicle rupturing agent Triton X-100 (0.15 mM). (c) Fluorescence emission spectra of Rho-B (λ_{max}(ex.) = 510 nm) at different time intervals. (d) Fluorescence emission spectra (λ_{max}(ex.) = 510 nm) of the release of entrapped Rho-B at different time intervals.

bonding with polar head groups, was used as the membrane-rupturing agent.[55] Rho-B-loaded vesicular self-assemblies of MGF, prepared in DMSO–H_2O (1 : 1 v/v, 0.15 mM), were treated with Triton X-100 (0.15 mM) and monitored using an epi-fluorescence microscope. Upon treatment, the rupture of the deep red colored dye-loaded vesicles was immediately observed, accompanied by the clear spreading of the fluorescent Rho-B molecules into the surrounding medium (Fig. 8b). Vesicle rupture was quantified using fluorescence emission spectroscopy over time. Rhodamine-B-loaded self-assemblies and Triton X-100 in DMSO–H_2O (1 : 1 v/v) were placed in a quartz cuvette (2 mm path length), and fluorescence emission intensities were measured (λ_{max}(em.) = 605 nm) at different time intervals after excitation at 510 nm. A gradual increase in the fluorescence emission intensity was observed (Fig. 8d). This increase directly correlates with the release of the entrapped Rho-B molecules into the bulk solution, confirming the lysis of the spherical self-assembly membranes by the surfactant. These experiments confirm the functional stability and controlled release capability of the MGF vesicles. They demonstrate the ability of the self-assemblies to effectively entrap a toxic dye and subsequently release it easily upon treatment with a membrane-rupturing agent (Triton X-100). This suggests their potential utility in controlled release applications.

Interestingly, 33.5% of rhodamine-B dye was released by the rapture of the Rho-B-loaded vesicular self-assemblies of mangiferin within 210 min (Fig. S19b).

3.3 Efficiency (%) of the entrapment and release of the anticancer drug doxorubicin

The entrapment of the anticancer drug doxorubicin (DOX) was studied by fluorescence emission experiments (λ_{max}(ex.) = 470 nm, λ_{max}(em.) = 600 nm).[56] A gradual decrease in the intensities of fluorescence emission was observed. The percentages of entrapment of DOX after 10, 25, 35, 50, 80 and 100 min were calculated to be 8.6%, 14.0%, 17.1%, 24.5%, 27.1%, and 32.5%, respectively (Fig. S20a). Similarly, a gradual increase in fluorescence emission intensity was observed by treating the doxorubicin-loaded self-assembled MGF with Triton-X 100. The percentage release of DOX after 10, 20, 35, 65, 75, 95 and 105 min was calculated to be 8.7%, 14.9%, 23.9%, 32.7%, 38.9%, 42.2%, and 55.6%, respectively (Fig. S20b).

3.4 Antibacterial activity study

Mangiferin is a polyphenolic xanthonoid containing the xanthone backbone and a glucoside unit. It has several biological and pharmacological activities such as anti-bacterial, anti-viral, anti-inflammatory, anti-allergic, antioxidant, anti-diabetic and anti-cancer activities.[57,58] It has different antimicrobial activities against bacterial strains such as *Escherichia coli*, *Staphylococcus aureus*, *Salmonella typhi* and fungi such as *T. aurantiacus* and *A. flavus*.[59] Due to its many alcoholic groups, it can damage the bacterial membrane, suppress biofilm formation and inhibit virulence factors.[36] It has low water solubility resulting in low bioavailability for various biological applications.

Curcumin is a polyphenol, belonging to the curcuminoid group, mainly responsible for the yellow color of turmeric produced from turmeric (*Curcuma longa*) plants. It has several medicinal activities such as anti-bacterial, anti-viral, anti-cancer, anti-inflammatory, anti-diabetic and antioxidant, and it is sold as a food coloring, food flavoring, herbal supplement and cosmetic ingredient.[60,61]

Curcumin is poorly soluble in water, and so it has low bioavailability for biological studies. This limited its uses in

Table 2 Inhibitory activity of the mangiferin (MGF)–curcumin mixture on *Staphylococcus aureus*[a]

Entry	Sample used	Inhibition zone diameter in mm (concentration of mangiferin/curcumin)
1	MGF in water	0 (1500 μg mL^{-1})
2	SA-MGF in DMSO–water (1 : 1)	0 (1500 μg mL^{-1})
3	Curcumin in DMSO	8 ± 0.50 (1500 μg mL^{-1})
4	SA MGF–curcumin (1 : 1) in DMSO–water (1 : 1)	10 ± 0.50 (1500 μg mL^{-1})

[a] SA = self-assembled, MGF = mangiferin, diameter of cork borer = 3 mm, solution mixtures added in every pit = 25 μL, and pathogen solutions added for spreading uniformly using a glass spreader on the agar gel surface = 100 μL.

Table 3 Inhibitory activity of the mangiferin (MGF)–curcumin mixture on *Escherichia coli*[a]

Entry	Sample used	Inhibition zone diameter in mm (concentration of mangiferin/curcumin)
1	MGF in water	0 (1500 μg mL^{-1})
2	SA-MGF in DMSO–water (1 : 1)	0 (1500 μg mL^{-1})
3	Curcumin in DMSO	8.00 (1500 μg mL^{-1})
4	SA MGF–curcumin (1 : 1) in DMSO–water (1 : 1)	8 ± 0.50 (1500 μg mL^{-1})

[a] SA = self-assembled, MGF = mangiferin, diameter of cork borer = 3 mm, solution mixtures added in every pit = 25 μL, and pathogen solutions added for spreading uniformly using a glass spreader on the agar gel surface = 100 μL.

medicinal and clinical research. To overcome the problems of low bioavailability and poor absorption of curcumin, we studied the entrapment of curcumin (1.36 mM) inside the vesicular self-assemblies of MGF in DMSO–H_2O (1 : 1 v/v, 17.76 mM) by epi-fluorescence microscopy. Interestingly, the bright red fluorescence was observed from the inner side of the vesicular self-assemblies under green emission light, indicating the entrapment of the curcumin inside the vesicles (Fig. S21).

Then, we examined the antibacterial activities of curcumin-loaded self-assembled MGF *via* a zone-inhibition method. We observed that at a concentration of 1500 μg mL^{-1}, only pure MGF in the water medium and self-assembled MGF in the DMSO–water (1 : 1 v/v) medium do not show any antibacterial activities against both Gram-positive bacteria (*Staphylococcus aureus*) and Gram-negative bacteria (*Escherichia coli*). Interestingly, curcumin loaded self-assembled MGF showed greater antibacterial activity than only curcumin in the DMSO–water (1 : 1 v/v) solvent system against both Gram-positive bacteria (*Staphylococcus aureus*) and Gram-negative bacteria (*Escherichia coli*) (Tables 2, 3 and Fig. S22).

The MIC values determined with curcumin by a micro-dilution method in the LB broth were 30 and 25 μg mL^{-1} for *S. aureus* and *E. coli* bacteria (Fig. S27a and b). With curcumin-loaded self-assembled MGF, the MIC values were determined to be 15 μg mL^{-1} for both *S. aureus* and *E. coli* bacteria, indicating enhanced antibacterial activities with curcumin-loaded self-assembled MGF (Fig. S23c and d). The MBC values determined with curcumin *via* a bacterial culture in Mueller–Hinton agar plates for 15 h inside an incubator at 37 °C were 50 μg mL^{-1} for both *S. aureus* and *E. coli* (Fig. S28a and b). With curcumin-loaded self-assembled MGF, the MBC values were determined to be 30 μg mL^{-1} and 35 μg mL^{-1} for *S. aureus* and *E. coli*, respectively, indicating enhanced antibacterial activities with curcumin-loaded self-assembled MGF (Fig. S28c and d).

The results clearly demonstrate that the vesicular self-assembly of MGF is an effective carrier system for hydrophobic antimicrobial agents like curcumin. By encapsulating curcumin, the system is likely to enhance its effective concentration, stability, and uptake by the bacteria, leading to superior antibacterial efficacy compared to curcumin administered in the same solvent alone.

4. Conclusions

In conclusion, the nano-sized mangiferin ($C_{19}H_{18}O_{11}$) is a natural polyphenolic xanthonoid compound containing the xanthone backbone and a glucoside unit. It forms vesicular self-assemblies in aqueous solvent and aqueous-organic binary liquid mixtures. The characterization for vesicular self-assemblies was carried out by optical microscopy, atomic force microscopy, scanning electron microscopy, high-resolution transmission electron microscopy and FTIR spectroscopy studies. Based upon the DFT calculation, FTIR spectroscopy, X-ray diffraction as well as HRTEM data, the bilayer-membrane formation model for the vesicular self-assembly of MGF was proposed. These vesicular self-assemblies are utilized for the entrapment of several toxic dyes and fluorophores such as anionic fluorophore carboxyfluorescene and cationic fluorophore rhodamine B including the anticancer drug doxorubicin. We also observed that the entrapped toxic dye rhodamine-B (Rho-B) was released from the vesicular self-assemblies of MGF on the treatment of the membrane-rupturing agent (Triton X-100). Thus, vesicles have the ability to entrap toxic dye and release it easily by the membrane rupturing agent. These vesicular self-assemblies were also used for the antibacterial studies. Curcumin-loaded vesicular self-assemblies of MGF showed greater antibacterial activity than only curcumin against both Gram-positive (*Staphylococcus aureus*) and Gram-

negative bacteria (*Escherichia coli*). The enhanced activity suggests that the self-assembled MGF significantly improves the solubility, stability and delivery of the MGF. Thus, the vesicular self-assembly of MGF has potential use as an important carrier system for toxic dye entrapment and release, drug delivery and anti-infective applications in several biological and medicinal fields.

5. Experimental

5.1 Extraction and isolation

5.1.1 Plant material. *Davallia solida* was collected from the Royal Project Foundation, Kasetsart University, Bangkok, Thailand in December 2015. Botanical identifications were made by Prof. M. L. Charuphant Thongtham, Department of Horticulture, Faculty of Agriculture, Kasetsart University, Bangkok, Thailand. The specimens were deposited at Chulabhorn Research Institute, Bangkok, Thailand as reference vouchers: CRI-Dso-RPF-Dec, 2015 (*D. solida*).

5.1.2 Isolation of mangiferin from *Davallia solida*. The dried rhizome of *Davallia solida* (1.19 kg) was soaked in MeOH (9 L × 3) at room temperature. Mangiferin (MGF, 4.81 g, 3.12% yield) was precipitated during the evaporation of MeOH extracts. The compound was purified by crystallization from ethanol and characterized by various spectroscopic techniques (Fig. S25–S28).

5.1.3 Self-assembly. First, the powdered solid of mangiferin **1** (MGF, generally 1–2 mg) was weighed in a series of dry vials and then dissolved in a certain amount of solvents by heating with magnetic stirring. Then the hot solution was cooled at room temperature and observed visually and using an optical microscope after 1–2 hours. For studying the self-assembly in organic-aqueous binary solvent mixtures, powdered solid of 1 was first solubilised in the neat organic liquid by heating and stirring. Then certain amount of water was added gradually, and the resulting mixture was heated with magnetic stirring. Then the solution was allowed to cool at room temperature and observed. Interestingly, we observed a colloidal solution and a viscous suspension in neat DMSO, EtOH, THF and water solvents. The viscous suspension was also observed in organic-aqueous binary solvent mixtures such as DMSO–H_2O, DMF–H_2O, THF–H_2O and EtOH–H_2O at different ratios and concentrations. Then, these colloidal and viscous solutions were used in several microscopic and spectroscopic studies to identify and characterize the self-assemblies of MGF (discussed earlier under the Results and discussion section).

Author contributions

SK: main contribution; conceptualization, investigation and manuscript writing. SP: investigation, conceptualization and manuscript writing. BGB: conceptualization, investigation, supervision, and manuscript preparation. WT: compound isolation, characterization and manuscript writing. CT: compound isolation, characterization, and manuscript writing. NT: compound isolation, characterization, and manuscript writing.

Conflicts of interest

The authors declare no competing interests.

Data availability

All data and models generated in this study appear in the submitted article or in the supplementary information (SI). Supplementary information: energy minimized structures of mangiferin, their isolation NMR and FTIR spectra, self-assembly studies, sample preparation method, histogram and morphological images from optical microscopy, and AFM, SEM, HRTEM, and X-ray diffraction (XRD) studies, the uses of the self-assemblies. See DOI: https://doi.org/10.1039/d6ra01279e.

Acknowledgements

WB-DSTBT grant no. STBT-11012(25)/9/2024-ST SEC and USIC of Vidyasagar University are acknowledged for the financial support and infrastructural facilities. SK acknowledges UGC for the research fellowship. NT would like to thank Thailand Science Research and Innovation (TSRI, grant number 53503/4821870) and the Chulabhorn Research Institute.

References

1 Y. Huang, C. Wu, J. Chen and J. Tang, *Angew. Chem., Int. Ed.*, 2024, **63**, e202313885.
2 G. M. Whitesides and M. Boncheva, *Proc. Natl. Acad. Sci. U. S. A.*, 2002, **99**, 4769–4774.
3 D. Pochan and O. Scherman, *Chem. Rev.*, 2021, **121**, 13699–13700.
4 S. Datta and S. Bhattacharya, *Chem. Soc. Rev.*, 2015, **44**, 5596–5637.
5 B. G. Bag, A. C. Barai, S. N. Hasan, S. K. Panja, S. Ghorai and S. Patra, *Pure Appl. Chem.*, 2020, **92**, 567–577.
6 S. Bhattacharya and S. K. Samanta, *Chem. Rev.*, 2016, **116**, 11967–12028.
7 X. Niu, E. J. Foster, B. O. Patrick and O. J. Rojas, *Adv. Funct. Mater.*, 2022, **32**, 2206058.
8 B. G. Bag and S. S. Dash, *Nanoscale*, 2011, **3**, 4564–4566.
9 S. Patra, S. Kar and B. G. Bag, *Chem.–Asian J.*, 2024, e20240036.
10 S. Patra, A. C. Barai, S. Kar S and B. G. Bag, *Biomass Convers. Biorefin.*, 2024, **15**, 6149–6161.
11 S. N. Hasan, J. Banerjee, S. Patra, S. Kar, S. Das, S. Samanta, D. Wanigasekera, U. Pavithra, K. Wijesekera, M. Napagoda, B. Giri, S. K. Dash and B. G. Bag, *Int. J. Biol. Macromol.*, 2023, **245**, 125416.
12 X. Niu, E. J. Foster, B. O. Patrick and O. J. Rojas, *Adv. Funct. Mater.*, 2022, **32**, 2206058.
13 B. G. Bag, S. Das, S. N. Hasan and A. C. Barai, *RSC Adv.*, 2017, **7**, 18136–18143.
14 Z. Jiang, X. Chen, Y. Lin, Q. Li, X. Nie, G. Xu, C. Yu, X. Zhang and Y. Luan, *Adv. Funct. Mater.*, 2023, **33**(1–15), 2307756.

15 X. Guo, W. Luo, L. Wu, L. Zhang, Y. Chen, T. Li, H. Li, W. Zhang, Ya. Liu, J. Zheng and Ya. Wang, *Adv. Sci.*, 2024, **11**, 2403388.
16 P. K. Vemula and G. John, *Acc. Chem. Res.*, 2008, **41**, 769–782.
17 B. G. Bag, S. Ghorai, S. K. Panja, S. K. Dinda and K. Paul, *RSC Adv.*, 2018, **8**, 29155–29163.
18 B. G. Bag and R. Majumdar, *Chem. Rec.*, 2017, **17**, 841–873.
19 K. S. Masters and S. Brase, *Chem. Rev.*, 2012, **112**, 3717–3776.
20 A. Matkowskia, P. Kus, E. Góralskaa and D. Wozniak, *Mini-Rev. Med. Chem.*, 2013, **13**, 439–455.
21 D. Z. Rechenchoskia, K. F. Agostinhoa, L. C. F. A. Galhardia, A. S. G. Lonnib, J. V. H. da Silvac, F. G. de Andradec, A. P. Cunhad, N. M. P. S. Ricardod, C. Nozawaa and R. E. C. Linharesa, *Bioorg. Med. Chem.*, 2020, **28**(1–6), 115304.
22 S. Meia, M. Perumala, M. Battinoc, D. D. Kittse, J. Xiaoc, H. Maa and X. Chen, *Crit. Rev. Food Sci. Nutr.*, 2023, **63**, 3046–3064.
23 T. B. Zou, E. Q. Xia, T. P. He, M. Y. Huang, Q. Jia and H. W. Li, *Molecules*, 2014, **19**, 1411–1421.
24 P. Talamond, L. Mondolot, A. Gargadennec, A. de Kochko, S. Hamon, A. Fruchier and C. Campa, *Acta Bot. Gallica*, 2008, **155**, 513–519.
25 T. Zou, H. Wu, H. Li, Q. Jia and G. Song, *J. Sep. Sci.*, 2013, **36**, 3457–3462.
26 T. H. T. Vo, T. D. Nguyen, Q. H. Nguyen and N. A. Ushakova, *Pharm. Chem. J.*, 2017, **51**, 44–48.
27 A. Dar, S. Faizi, S. Naqvi, T. Roome, S. Z. U. Rehman, M. Ali, S. Firdous and S. T. Moin, *Biol. Pharm. Bull.*, 2005, **28**(4), 596–600.
28 J. C. Barreto, M. T. S. Trevisan, W. E. Hull, G. E. Erben, S. De Brito, B. Pfundstein, G. B. Spiengelhalder and R. W. Owen, *J. Agric. Food Chem.*, 2008, **56**, 5599–5610.
29 Y. W. Liu, X. Zhu, L. Zhang, Q. Lu, J. Y. Wang, F. Zhang, H. Guo, J. L. Yin and X. X. Yin, *Eur. J. Pharmacol.*, 2013, **721**, 355–364.
30 Y. Niu, W. Lu, L. Gao, H. Lin, X. Liu and L. Li, *Pharm. Biol.*, 2012, **50**, 1177–1182.
31 S. Saha, P. Sadhukhan and P. C. Sil, *Biofactors*, 2016, **42**, 459–474, DOI: 10.1002/biof.1292.
32 B. Zhang, J. Fang and Y. Chen, *Lett. Drug Des. Discovery*, 2013, **10**, 239–244.
33 S. N. Morozkina, T. H. N. Vu, Y. E. Generalova, P. P. Snetkov and M. V. Uspenskaya, *Biomolecules*, 2021, **11**, 79.
34 S. K. Singh, R. M. Tiwari, S. K. Sinha, C. C. Danta and S. K. Prasad, *Asian Pac. J. Trop. Biomed.*, 2012, S884–S887.
35 R. S. Yehia and S. A. Altwaim, *Plants*, 2023, **12**, 1539.
36 P. Serbun, R. Shaikenov, V. Klimshina, S. Morozkina and P. Snetkov, *Eng. Proc.*, 2025, **87**(1–15), 58.
37 M. Telang, S. Dhulap, A. Mandhare and R. Hirwani, *Expert Opin. Ther. Pat.*, 2013, **23**, 1561–1580.
38 H. Iqbal, M. Inam-Ur-Raheem, S. Munir, R. Rabail, S. Kafeel, S. Arashi, A. M. Khaneghah and R. M. Aadil, *Food Sci. Nutr.*, 2024, **12**, 1413–1429.
39 I. Shaikh and H. K. Tatapudi, *Discov. Chem.*, 2025, **2**(1–16), 115.
40 Z. W. Yu and P. J. Quinn, *Biosci. Rep.*, 1994, **14**, 259–281.
41 A. Pielesz, A. Gawłowski, D. Biniaś, R. Bobiński, M. Kawecki, A. Klama-Baryła, D. Kitala, W. Łabuś, J. Glik and J. Paluch, *Spectrochim. Acta, Part A*, 2018, **196**, 344–352.
42 *DFT (Density Functional Theory) using Gaussian 09 software, B3LYP and 6-31G basis set*.
43 *PC Model version 9.2 (Serena Software)*.
44 Cambridge Crystallographic Data Centre, 2025, *Free Mercury*, CCDC, https://www.ccdc.cam.ac.uk/solutions/software/free-mercury.
45 M. Li, H. J. Wang, D. M. Wu, *Experimental Crystal Structure Determination*, 2021, CCDC, https://www.ccdc.cam.ac.uk/structures/Search.Ccdcid=819495&Database.
46 S. Yang, Q. Zhou, B. Zhang, L. Zhang, D. Yang, H. Yang and Y. Lu, *Nat. Prod. Bioprospect.*, 2020, **10**, 187–200.
47 J. W. da Cruz Jr, L. R. d. Moraes, M. H. d. Santos, G. A. d. Silva, M. R. P. L. Brigagao, J. Ellena and A. C. Doriguetto, *Helv. Chim. Acta*, 2008, **91**, 144–154.
48 S. K. Panja, K. D. Wijesekera, M. T. Napagoda, B. G. Bag and B. G. Prayogik, *Rasayan*, 2018, **2**, 5–8.
49 T. Shimizu, M. Masuda and H. Minamikawa, *Chem. Rev.*, 2005, **105**(4), 1401–1443.
50 R. Majumdar and B. G. Bag, *RSC Adv.*, 2014, **4**, 53327–53334.
51 B. G. Bag, S. N. Hasan, S. Ghorai and S. K. Panja, *ACS Omega*, 2019, **4**, 7684–7690.
52 W. Cui, J. Li and G. Decher, *Adv. Mater.*, 2016, **28**, 1302–1311.
53 B. G. Bag, C. Garai and S. Ghorai, *RSC Adv.*, 2019, **9**, 15190–15195.
54 S. Ghorai and B. G. Bag, *ChemistrySelect*, 2020, **5**, 15032–15038.
55 D. Koley and A. J. Bard, *Proc. Natl. Acad. Sci. U. S. A.*, 2010, **107**, 16783–16787.
56 B. G. Bag, S. N. Hasan, S. Ghorai and S. K. Panja, *ACS Omega*, 2019, **4**, 7684–7690.
57 S. K. Singh, R. M. Tiwari, S. K. Sinha, C. C. Danta and S. K. Prasad, *Asian Pac. J. Trop. Biomed.*, 2012, S884–S887.
58 N. A. Mazlan, S. Azman, N. F. Ghazali, P. Z. S. Yusri, H. M. Idi, M. Ismail and M. Sekar, *Drug Invent. Today*, 2019, **12**, 14–17.
59 A. H. Madhagi, *Nanotechnol., Sci. Appl.*, 2025, **18**, 277–294.
60 J. S. Rad, Y. E. Rayess, A. A. Rizk, C. Sadaka, R. Zgheib, W. Zam, S. Sestito, S. Rapposelli, K. N. Skocińska, D. Zielińska, B. Salehi, W. N. Setzer, N. S. Dosoky, Y. Taheri, M. E. Beyrouthy, M. Martorell, E. A. Ostrander, H. Suleria, W. C. Cho, A. Maroyi and N. Martins, *Front. Pharmacol*, 2020, **11**(1–23), 01021.
61 C. Dai, J. Lin, H. Li, Z. Shen, Y. Wang, T. Velkov and J. Shen, *Antioxidants*, 2022, **11**(1–21), 459.